Quantitative X-ray spectroscopy of massive stars

L.M. Oskinova[a], W.-R. Hamann[a], A. Feldmeier [a]

[a]Potsdam University, Am Neuen Palais 10, Potsdam, 14469 Germany

Radiative transfer in a clumped winds is used to describe X-ray emission line profiles observed in the *XMM-Newton* RGS spectrum of the OI star ζ Puppis. It is shown that this X-ray spectrum can be explained as originating from a multi-temperature collisional plasma located in the wind acceleration zone. The X-rays are attenuated in the clumped stellar wind, which gives characteristic profiles to the emergent lines. We specifically study the N VII emission line in the spectrum of ζ Pup. Long RGS exposures reveal that the N VII line profile is structured. On the basis of our ζ Pup atmosphere model, we rule out the presence of N VII in the cool wind component. We suggest that the detailed N VII line structure is due to self-absorption in the hot plasma. Wind clumping also affects the transfer of ionizing radiation in high-mass X-ray binaries (HMXBs). We derive analytical formulae for the ionisation parameter in dependence on the parameters of wind clumping.

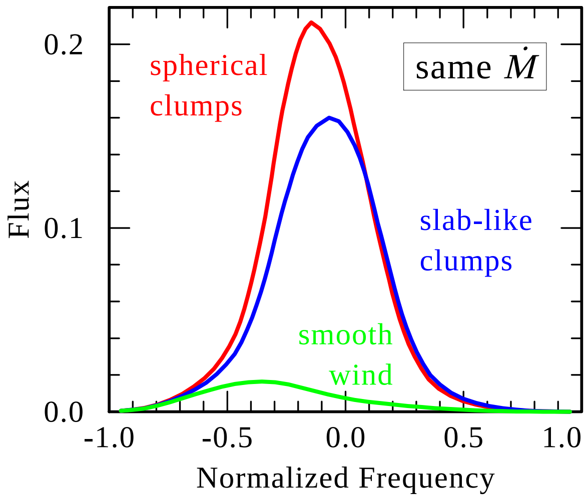

Figure 1. Model X-ray emission line profiles. The same stellar parameters were assumed for all three profiles, except of different clumping properties as indicated.

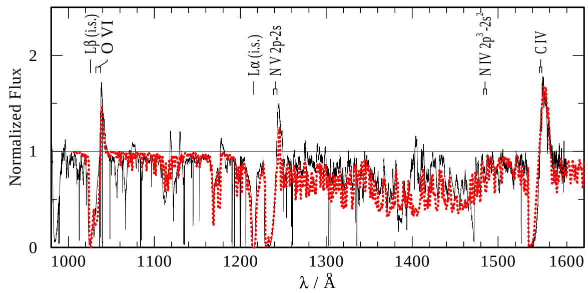

Figure 2. The EUV spectrum of ζ Pup, observed with FUSE (thin line), compared to a PoWR model spectrum (dotted). The resonance doublets of C IV, N V and O VI are well reproduced, as well as the "forest" of iron-group lines. The O VI doublet can only be fitted with models when assuming that a diffuse X-ray field causes additional ionisation.

1. Clumping of the stellar wind

Stellar winds of O-type stars are strongly clumped as confirmed by the growing number of observational evidences. The observed variability in the He II 4686 Å emission line in ζ Pup was explained as an excess emission from the wind clumps [1]. The Hα variability in a large sample of O stars was reproduced by a wind model consisting of coherent shells [2].

The empirical mass-loss estimates shall be generally reduced by factors of a few in clumped winds [3]. From a study of FUV spectra of 40 Galactic O-stars it was concluded that their mass-loss rates should be reduced by up to one order of magnitude due to wind clumping [4]. An analysis of the X-ray emission line profiles from δ Ori, ζ Pup, and ζ Ori [5–7] has shown that the attenuation by the stellar wind is significantly smaller than expected from homogeneous wind models. The observed attenuation of X-rays in the massive binary γ^2 Vel is much weaker than expected from smooth stellar wind models, implying strong wind clumping [8]. Similar conclusions were reached

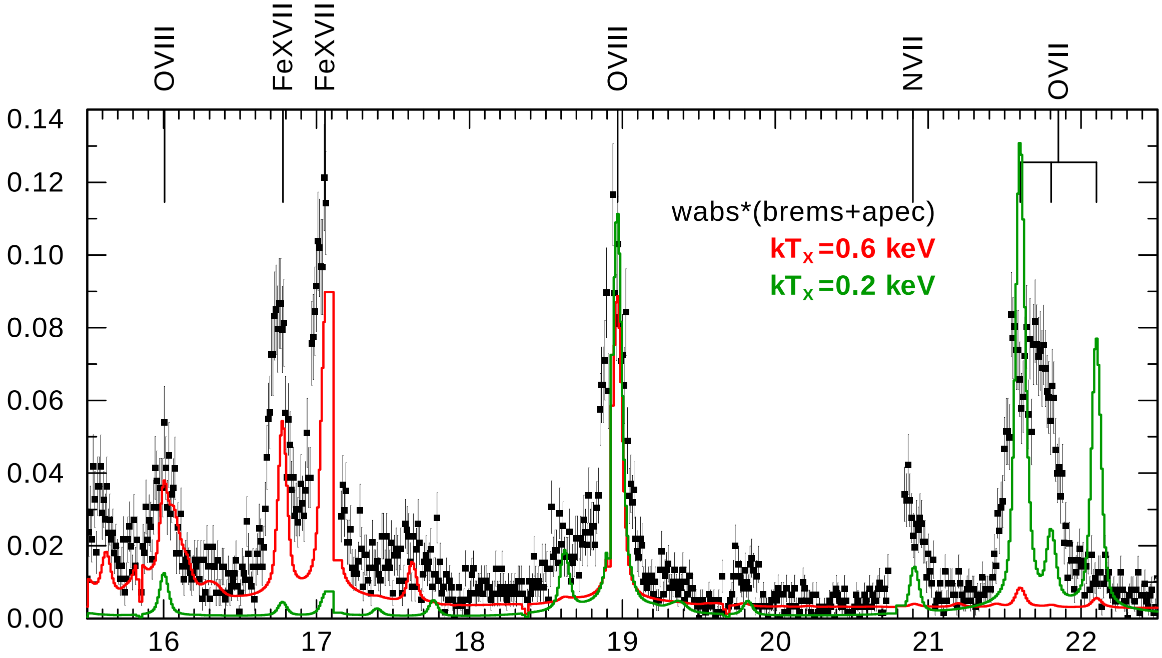

Figure 3. Part of *XMM-Newton*RGS spectrum of ζ Pup. Overplotted are two *wabs*$\times$*apec* models with different temperatures. The level of continuum and the line ratios are in agreement with a plasma in collisional equilibrium.

from the X-ray observations of WR 140 [9].

The X-ray emission line spectra of several wind-fed high-mass X-ray binaries (HMXB) can be explained as originating in a wind where cool dense clumps are embedded in rarefied photoionized gas [10]. The stochastic variability of X-ray lightcurve observed by *XMM-Newton* in 4U 1700-37 were explained as the result of the neutron star feeding by a strongly clumped stellar wind [11].

Clumping of the stellar wind is thought to be a consequence of the intrinsic instability of the radiative-driving mechanism [12]. The 1D hydrodynamic modeling predicts that line-driven stellar winds are strongly inhomogeneous, starting from close to the photosphere [13]. Strong gas compression leads to the formation of cool clumps. The space between clumps is essentially void, but small gas parcels are ablated from the clumps and accelerated to high speed. When a parcel catches up and rams into the next outer clump, the gas is heated and emits thermal X-rays. The X-rays propagate trough the wind and suffer absorption by the cool clumped component of the wind. gets. Thus the wind consists of two disjunctive components: hot ($\sim 10^7$ K) gas parcels emitting X-rays and compressed cool ($\sim 10^5$ K) fragments that attenuate this radiation.

Radiative transfer in a clumped wind is different from transfer in a homogeneous wind [14]. Formation of X-ray emission lines in clumped winds of massive stars was extensively studied in [15–17]. The main findings of these studies are

- The opacity in a clumped wind is reduced compared to a homogeneous wind of the same mass-loss rate.

- The wavelength-dependence of the opacity is weaker in clumped winds; if clumps are optically thick, the opacity becomes grey.

- X-ray emission line profiles are nearly symmetric and have similar shapes across the spectrum.

- The line profiles observed in X-ray spectra of single O stars can be reproduced in the framework of a clumped wind model.

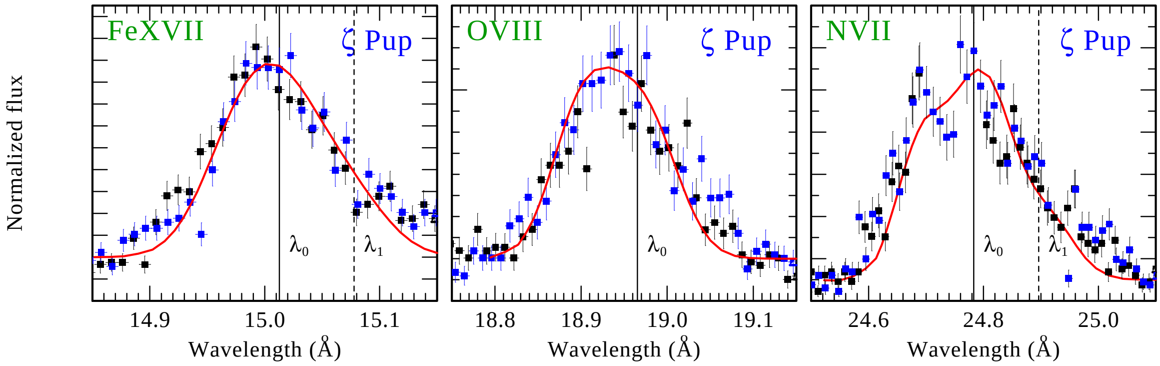

Figure 4. Lines observed in ζ Pup (overplotted are RGS1 and RGS2). The solid lines are the clumped wind model with $\dot{M} = 8.8 \times 10^{-6}\, M_\odot\, \mathrm{yr}^{-1}$. The cool-wind opacity is calculated from a PoWR model. The rest-frame wavelength is denoted λ_0. The rest-frame wavelengths of blended lines are denoted λ_1.

Fig. 1 shows model line profiles for smooth and clumped winds. Two models of clumped wind are shown: the wind which consists of the spherical and of the flattened clumps. The line flux in the Fig. 1 is normalized such that it is unity for a line which is not affected by absorption. As can be seen from Fig. 1 the emergent flux in the line is lower in a smooth wind that in a clumped wind model. It is assumed that the total number of clumps in the wind is constant. Clumps form at random times near some inner boundary and propagate radially according to a monotonically increasing velocity law. An average time separation between clumps is equal to the wind flow time $T_{\rm fl} = R_*/v_\infty \sim 1\,$hr. The line profiles are affected by the assumed clump geometry. A model with spherical clumps assumes that the optical depth across a clump has no angular dependence (see [18]). Slab-like clump models assume clumps, that are geometrically thin and aligned. In the latter model the optical depth across the clump is angular-dependent (see [15–17]) and the resulting line profile is more symmetric. Future 2D hydrodynamic models will shed new light on the clump geometry.

2. Stellar atmosphere model

While our 2D clumped-wind model is used to calculate the formal radiative transfer, the opacity of the cool medium is obtained with the Potsdam Wolf-Rayet (PoWR) non-LTE code [1]. Shown in Fig. 2 is the observed FUSE spectrum of ζ Pup with overplotted model. The model and observations are flux-calibrated. An X-ray field of the observed level has been included in the model to fit the observations. As can be seen in Fig. 2 the P Cyg line profile of O VI is nicely reproduced by the model. It was the presence of such high ions as O VI observed in O-star spectra, which led Cassinelli & Olson [19] to postulate the presence of X-rays in stellar winds, prior to their actual discovery. In agreement with this classical work, our state-of-the-art model cannot reproduce the observed O VI line unless in the presence of X-rays.

The scattering by the resonance O VI line in the wind is needed to be taken into account for the analysis of the $\mathcal{R}$ ratio between forbidden and intercombination lines in helium-like Mg XI [20]. The transition between $2^3S_1 \rightarrow 2^3P_1$ levels at $\lambda\,1034.31\,$Å is between O VI doublet at $\lambda\,1031.91$ Å and $\lambda\,1037.61\,$Å. Thus, the full radiative transfer is needed to evaluate the effect of radiation field on the lines ratio in helium-like ions. This is fully accounted for in our atmosphere models.

From the line ratios in helium-like ions observed by *Chandra* and *XMM-Newton* in ζ Pup we infer the X-ray formation region to be located approximately between $1.5\,R_*$ and $10\,R_*$ [17]. This is consistent with the radii of formation obtained

[1] www.astro.physik.uni-potsdam.de/~wrh/PoWR/powrgrid1.html

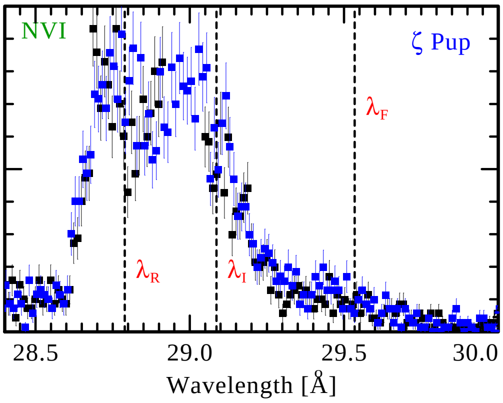

Figure 5. Observed N VI line in spectrum of ζ Pup.

independently from line profile fits. Detailed analysis of the forbidden-to-intercombination line ratios in ζ Pup, ζ Ori, ι Ori, and δ Ori is presented in [20].

3. Analysis of *XMM-Newton* RGS spectrum of ζ Pup

We have analyzed the archival RGS spectra of ζ Pup. General properties of ζ Pup's X-ray spectrum are consistent with a multi-temperature plasma in collisional equilibrium (CIE), as confirmed by a study of differential emission measure distribution [21]. Fig. 3 shows part of the RGS spectrum with overplotted *wabs*apec* CIE models for two temperatures. As can be seen, the ratio of O VIII Lyβ(λ16.20)/Lyα(λ18.99) is consistent with a plasma temperature of $kT_{\rm X} \approx 0.6$ keV. On the other hand, the strength of O VII helium-like line indicates presence of a $kT_{\rm X} \approx 0.2$ keV plasma. Importantly, the level of continuum seen in this high quality spectrum is in agreement with the inferred plasma temperatures.

Continuum was only marginally detected in previous less sensitive observations [22] and its alleged weakness was used as an argument to support the idea, that the shocks in O star winds are collisionless (Rauw, Pollock & Nazé, these proceedings). A recent study of collisionless damping in stellar winds shows that in rotating magnetized stars this mechanism can indeed be important [23]. However, from both dynamic and energetic arguments it was demonstrated that it

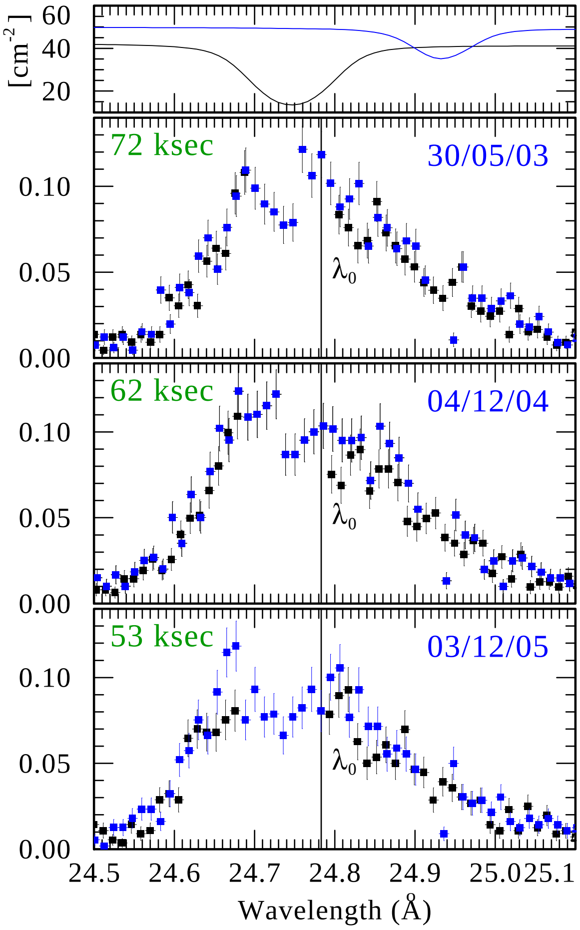

Figure 6. Observed N VII lines in spectrum of ζ Pup (RGS1 and RGS2 are overplotted). The upper panel shows the sensitivity areas of RGS1 and RGS2 across the line. The exposure time and the date of observation are in left and right upper corners.

can operate effectively only in stars with spectral type B3V or later, but not in O stars [23].

In order to fit the observed line profiles we have added the observed level of continuum to the model lines. Fig. 4 shows the most prominent emission lines in the RGS spectrum. The model lines were obtained with our 2D clumped wind model [16]. The region of X-ray line formation is constrained from an analysis of the *fir* line ratios in He-like ions [17,20]. Therefore, the only free parameter in the modeling is the *fragmentation frequency*. Our model assumes time averaged sta-

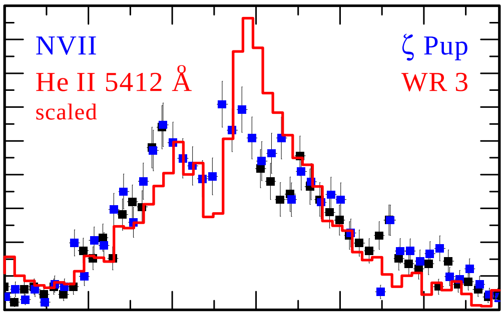

Figure 7. Comparison between the shape of the optically thick He II line observed in WR 3 and the N VII in the X-ray spectrum of ζ Pup.

tionary mass-loss rate and the average number of clumps in the wind at a given moment of time is constant. The fragmentation frequency is an inverse time interval at which moving clumps are crossing some arbitrary reference radius in the wind [17]. We prefer to use this parameter instead of *porosity length* [18], since the latter is radius-dependent whereas the former is not.

The model lines shown in Fig. 4 are obtained using mass-loss estimate which does not account for wind clumping [24]. The fragmentation frequency for all models is $10^{-4}\,\mathrm{s}^{-1}$. This corresponds to the inverse flow time, $T_{\rm fl} = v_\infty/R_*$, in the wind of ζ Pup. Using more realistic mass-loss rates that are smaller by a factor of few will result in slightly higher fragmentation frequency. The Fe XVII (λ15.01) line is wide and cannot be satisfactorily fitted unless the line formation region extends further out in the wind. We assumed here that the line is blended with Fe XIX. The emissivity of Fe XIX (λ15.08) is about 30% of Fe XVII (λ15.01), assuming a temperature $kT_{\rm X} \sim 0.7$ keV. In the most red part of the wing of Fe XVII, the emission from O VIII (λ15.17) is also likely to contribute.

The O VIII (λ18.97) is easily fitted with the present model of a clumped wind.

Several authors have noted that the profile of N VII (λ24.785) is different from that of other lines [22,25]. It was recently suggested that this line is blended with N VI (λ24.898) [26]. Following this suggestion we model N VII line as a blend. Assuming ionisation equilibrium, the ratio of N VI to N VII is sensitive to the temperature. Fig. 5 shows the observed N VI triplet line. The measured ratio $\mathcal{G} = f + i/r = 1.1 \pm 0.1$ corresponds to a temperature $T_{\rm X} \approx 1$ MK [27]. At this temperature, the emissivity of N VI (λ24.898) is half of the emissivity of N VII (λ24.785) (ATOMDB v.1.3.1). Using these values in clumped wind model, the resulting fit satisfactorily reproduces the N VII line width, as is shown in Fig. 4.

Figure 6 shows three different *XMM-Newton* observations of the N VII line and the sensitivity areas of RGS1 and RGS2. The "ragged" structure of the line profile and the dip at λ24.74Å is clearly seen in all data sets. While the depth of the dip is variable, its location is relatively constant.

We employed PoWR model to study whether the absorption in the cool wind can cause the observed structure of the N VII line. N VII can be produced in the cool wind via Auger ionisation of N V. However, our atmosphere models show that N VII is absent in the cool wind, even when assuming that the X-ray field is significantly stronger in ζ Pup wind than observed.

The line structure seen in N VII is typical for the optically thick lines in the winds of hot stars. Fig. 7 shows the optically thick He II line in the spectrum of WR 3, overplotted with the N VII line in ζ Pup's spectrum. The optical depths in the resonance lines of the most abundant ions in the hot X-ray emitting component of stellar winds can be larger than unity [28]. Nitrogen is overabundant in ζ Pup, while oxygen and carbon are depleted. We find that the optical depth in N VII line can be large enough to result in self-absorption.

4. The photoionisation parameter in the clumped wind of HMXBs

Clumping of the stellar wind has a profound effect on X-ray emission from HMXBs [10]. We studied the influence of clumping on photoionised regions. In the following we consider the case of optically thick clumps. The same notations as in [29] are used. We assume that the wind consists of two components: dense clumps and a rarefied interclump medium. Applying the continuity equation we define the mean particle number density as

$$n(r_*) \equiv \frac{\dot{M}}{4\pi\mu m_{\rm H} v(r_*) r_*^2}, \qquad (1)$$

where μ is mean molecular weight and $m_{\rm H}$ is the atomic mass unit. If the density enhancement in clumps is $D = <n^2>/<n>^2$, and the volume filling factor of clumps is $f_{\rm V}$ then the particle number density of the interclump gas is

$$n_{\rm ic} = (1 - Df_{\rm V})n \qquad (2)$$

Assume for simplicity that the interclump gas is optically thin and the velocity is constant. Correcting the mean radiation intensity for the absorption in the clumps

$$J_\nu = \frac{L_{\rm X}}{4\pi r_*^2} \cdot f(kT) \cdot {\rm e}^{-\bar{\tau}(r_*)}, \qquad (3)$$

where $f(kT)$ is a function of atomic parameters and temperature, and $\bar{\tau}$ is an effective optical depth. When all clumps are opaque ($\tau_{\rm clump} \gg 1$), the effective optical depth reflects geometrical distribution of the clumps, and is found to be grey [15,16]

$$\bar{\tau} = \frac{n_0 r_*}{v} \qquad (\text{if} \quad \tau_{\rm clump} \gg 1), \qquad (4)$$

where n_0 is the fragmentation frequency. Using the ionisation balance equation, the ionisation parameter in the interclump medium is

$$\xi = \frac{L_{\rm X}}{\langle n \rangle r_*^2} \cdot \frac{{\rm e}^{-\bar{\tau}}}{1 - Df_{\rm V}}. \qquad (5)$$

For a very high fragmentation frequency, which recovers the case of a smooth wind $Df_{\rm V} \approx 0$, Eq. 5 reduces to the usual definition of ξ. Parameter q [29] in a clumped wind can be written as

$$q = \frac{r_*^2}{r_{\rm X}^2} \cdot {\rm e}^{-\bar{\tau}}. \qquad (6)$$

We conclude that clumping affects both the ionisation balance and the size of the photoionized region.A higher ionisation and a larger size of the photoionized region can be expected.

REFERENCES

1. Eversberg, T., Lèpine, S., Moffat, A.F.J . 1998, ApJ, 494,799
2. Markova, N., Puls, J., Scuderi, S., Markov, H. 2005, A&A, 440, 1133
3. Hamann, W.-R. & Koesterke, L. 1998, A&A, 335, 1003
4. Fullerton, A.W., Massa, D.L., Prinja, R.K. 2006, ApJ, 637, 1025
5. Miller, N.A., Cassinelli, J.P., Waldron, W.L., *et al.* 2002, ApJ, 577, 951
6. Kramer, R.H., Cohen, D.H., Owocki, S.P. 2003, ApJ, 592, 532
7. Cohen, D., Leutenegger, M.A., Grizzard, K.T., *et al.* 2006, MNRAS, in press, astro-ph/0602599
8. Schild, H. *et al.* 2004, A&A, 422, 177
9. Pollock, A.M.T., Corcoran, M.F., Stevens, I.R. *et al.* 2005, ApJ, 629, 482
10. Sako M., Kahn S.M., Paerels F., *et al.* 2003, in High Resolution X-ray Spectroscopy with *XMM-Newton* and *Chandra*, ed. G. Branduari-Raymont (astro-ph/p309503)
11. van der Meer, A., Kaper, L., Di Salvo, T., *et al.* 2005, A&A, 432, 999
12. Lucy L.B. & Solomon P.M., 1970, ApJ, 159, 879
13. Feldmeier, A., Puls, J., Pauldrach, A.W.A. 1997, A&A, 322, 878
14. Pomraning G.C., 1991, Linear kinetic theory and particle transport in stochastic mixtures, Singapore; New Jersey: World Scientific. Series on advances in mathematics for applied sciences 7
15. Feldmeier, A., Oskinova, L., Hamann, W.-R. 2003, A&A, 403, 217
16. Oskinova, L.M., Feldmeier, A., Hamann, W.-R. 2004, A&A, 422, 675
17. Oskinova, L.M., Hamann, W.-R., Feldmeier, A. 2006, MNRAS, submitted, astro-ph/0603286
18. Owocki S.P. & Cohen D.H., 2006, ApJ, in press, astro-ph/0602054
19. Cassinelli, J.P. & Olson, G.L. 1979, ApJ, 229, 304
20. Leutenegger, M.A., Paerels, F.B.S., Kahn, S.M., Cohen, D.H., 2006, ApJ, submitted
21. Wojdowski, P.S. & Schulz, N.S. 2005, ApJ, 627, 953
22. Kahn S.M., Leutenegger M.A., Cotam J., *et al.* 2001, A&A, 276, 117
23. Suzuki, T.K., Yan, H., Lazarian, A., Cassinelli, J.P. 2006, ApJ, 640, 1005
24. Repolust, T., Puls, J., Herrero, A., 2004, A&A, 415, 349
25. Cassinelli J.P., Miller N.A., Waldron W.L., *et al.* 2001, ApJ, 554, L55
26. Pollock, A.M.T. & Raassen, A.J.J. 2006, A&A, submitted
27. Porquet D., Mewe R., Dubau J., *et al.* 2001, A&A, 376, 1113
28. Ignace, R. & Gayley, K.G. 2002, ApJ, 568, 954
29. Hatchett, S. & McGray, R. 1977, ApJ, 211, 552

ACKNOWLEDGEMENTS

Based on observations obtained with *XMM-Newton*, an ESA science mission with instruments and contributions directly funded by ESA Member States and NASA. LMO and AF acknowledge support from DFG grant Fe 573/2-1.